

Radar Guided Dynamic Visual Attention for Resource-Efficient RGB Object Detection

Hemant Kumawat

*School of Electrical and Computer Engineering
Georgia Institute of Technology
hkumawat6@gatech.edu*

Saibal Mukhopadhyay

*School of Electrical and Computer Engineering
Georgia Institute of Technology
saibal.mukhopadhyay@ece.gatech.edu*

Abstract—An autonomous system’s perception engine must provide an accurate understanding of the environment for it to make decisions. Deep learning based object detection networks experience degradation in the performance and robustness for small and far away objects due to a reduction in object’s feature map as we move to higher layers of the network. In this work, we propose a novel radar-guided spatial attention for RGB images to improve the perception quality of autonomous vehicles operating in a dynamic environment. In particular, our method improves the perception of small and long range objects, which are often not detected by the object detectors in RGB mode. The proposed method consists of two RGB object detectors, namely the Primary detector and a lightweight Secondary detector. The primary detector takes a full RGB image and generates primary detections. Next, the radar proposal framework creates regions of interest (ROIs) for object proposals by projecting the radar point cloud onto the 2D RGB image. These ROIs are cropped and fed to the secondary detector to generate secondary detections which are then fused with the primary detections via non-maximum suppression. This method helps in recovering the small objects by preserving the object’s spatial features through an increase in their receptive field. We evaluate our fusion method on the challenging nuScenes dataset and show that our fusion method with SSD-lite as primary and secondary detector improves the baseline primary yolov3 detector’s recall by 14% while requiring three times fewer computational resources.

Index Terms—Object Detection, Radar, RGB Camera, Sensor Fusion, Autonomous Systems, Deep Learning

I. INTRODUCTION

Object detection is one of the most challenging tasks in autonomous systems. Deep convolutional architectures such as R-CNN [1], Fast R-CNN [2], and Faster RCNN [3] provide very high accurate object detection results. However, due to slow inference time and high memory requirements [4], single stage detectors like SSD [5] and YOLO [6] are used for faster detection often at a slightly lower accuracy. However, single stage RGB detectors suffer from degradation in performance on small object detection task. Object detection becomes very challenging as the object height relative to the image size decreases [7]. In addition to this, these object detectors perform very poorly when they are exposed to novel environments or adverse lighting and weather conditions [8] [9]. These perception failures could be very critical to the autonomous system’s decision making module and may cause catastrophic failures.

To overcome the limitations of RGB camera based perception, modern day autonomous systems are often equipped with multiple perception modalities like cameras, radars, and LiDARs [10] [11]. Using multiple sensors allows the perception engine of the autonomous systems to exploit complementary features provided by different modalities. Automotive radars have been widely used in vehicles for Advanced Driving Assistance Systems (ADAS) [12] as they can detect long range objects and are highly robust to adverse weather and lighting conditions. Hence, a radar could provide valuable information of long range objects that are missed by the RGB detectors.

Although radar could detect objects at long range accurately, processing radar point cloud is a very challenging problem due to the unstructured nature of the data. The radar’s pointcloud is very sparse with inconsistent point density for objects without any labels. Classical methods [13] [14] [15] for fusing camera and radar includes kinetic model based tracking and filter based association algorithms. However, noisy and sparse 3D radar data makes the association problem challenging. Often this process is handcrafted with some heuristic rules to make it work with 2D RGB images. An emergent solution is to use radar point based feature extraction methods. These methods are usually designed for dense LiDAR pointclouds such as PointNet [16] and hence do not have a good performance on sparse and noisy radar data. Other methods include creating a depth map using raw radar data and then fusing the depth map with RGB images [17] [18]. However, many of these methods require two stage detectors [19] making them computationally expensive for resource constrained systems. Even though methods with radar guided feature extraction have better results on small object detection, they are far from real time deployment on robotics systems due to their high computational needs.

This paper introduces a novel fusion method for RGB camera and radar to detect small and far away objects in RGB images with low complexity and memory footprint. The proposed method is designed with a lightweight single stage detector that fuses radar point cloud with RGB images to generate ROIs for object candidates. Radar point cloud contains range, azimuthal and velocity information of objects with high confidence. Each point in the radar pointcloud when projected onto the image plane gives an approximate location of the object in the image. We use radar points to generate

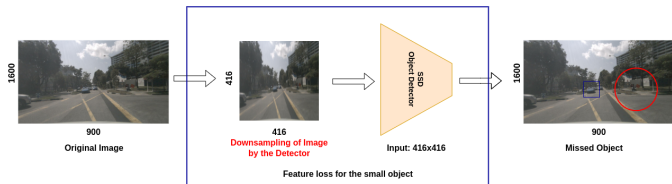


Fig. 1: Feature loss for small object

regions of interests with object candidates. These ROIs are fed to the lightweight detector to generate object detections. This increases the relative size of the object with respect to the ROI image and thereby, reducing the information loss of object features while convolution and pooling operations. The final step includes a fusion of these detections with detections made by passing the full image to another detector using NMS. This way we recover any large objects missed or not fully detected due to cropping of the image. We refer to this network as 'Primary detector' and our lightweight detector as 'Secondary detector'. We evaluate our network on the nuScenes dataset [20] which provides synchronized data from a full autonomous sensor suite including multiple radars and RGB cameras. Our experiments show that the proposed method shows 14% increase in recall for fusion system with SSDlite [21] as primary and secondary detector than baseline yolov3 detector while only requiring 22.3 GFLOPs against 66.4 GFLOPs of the primary detector.

II. FUSION FRAMEWORK

A. Motivation

Our understanding of how well the current object detectors perform on detection task is largely measured by observing average recall and precision on benchmark datasets. However, there is a big gap between the detectors' performance on small and large objects which is not reflected in average performance numbers. This is true for any type of object detector and this gap increases for detectors with a small computational footprint [22] [23]. The small objects in the images lack the distinctive features and when passed through the convolutional backbone of the network, background and nearby pixel features begin to dominate in higher layers as shown in figure 1. Low level features generated using lower layers do not have enough semantic information to help in prediction which makes this problem very challenging.

One of the ways to increase the receptive field of the small object is to scale the image to a large size and then pass it through the detector. This reduces the feature corruption for the object with background and nearby pixels, thereby helping in better performance on small objects. Authors in [24] use two object detectors for the face detection task with a second detector processing the upscaled image to detect small objects. However, increasing the input size for detectors increases the computational overhead of the system significantly making it impractical for systems with limited computational power. Table I shows the effect of increasing the input scale for yolov3-spp on recall and GFLOPs. We observe an increase

TABLE I: Comparison between performance and computation overhead for yolov3 with different input size

Image size	Recall	GFLOPs
256	0.29	25.1
416	0.42	66.4
512	0.45	100.5
640	0.49	157.1
1080	0.54	447.4
1920	0.49	1413.9

in recall of the detected objects as the input size is increased from 256 to 1080, however it increases the computational load by almost 17 times. Note that the relation between the number of GFLOPs and input size is not linear and it increases non-linearly as the input size is scaled.

The receptive field for the small object could also be increased by cropping a small region around the object and passing it through the detector. This increases the normalized area of the object pixels relative to the cropped image thereby reducing the feature loss to the background and nearby pixels. However, single detectors are not designed to create proposals for the object regions. In absence of proposal generators for object regions [7], many works try to divide the image into multiple tiles and pass them through the detector. However, this design may require a large number of regions created randomly in the image to detect all the small objects. This may severely affect the computational efficiency of the network leading to a higher inference time.

Radar's power of detecting objects at long range could be very helpful in guiding where the object is in the image. Radar detection when mapped to the image gives an approximate location of the object which could be used to create proposals for the object regions. Many of the automotive radars have very sparse data with less than 64 points making them excellent for our purpose. There have been prior works where the radar data is used to guide the proposal generation stage in two stage detectors [25] [26]. Yadav et. al [19] created a network BIRANet which fused radar points with a feature extractor network to guide anchors generation for Faster R-CNN. However, the anchors generated using this method do not increase the receptive field and only act as a proposal generator. Moreover, they require high energy resources and have a longer inference time due to the use of two stage detectors.

B. Proposed Architecture

In this study, we aim to use the radar points to generate object proposals in the image and use lightweight detectors to detect objects in the proposal regions. Our proposed fusion network is shown in Figure 2. The proposed network consists of two detectors: a primary detector and a secondary lightweight detector. The primary detector takes the RGB images and generates detection for the full image. We refer to these detections as primary detections. Next, the radar points are projected to the RGB image frame to generate object proposals. These object proposals regions of a predefined size are cropped from the image and each of them is sent

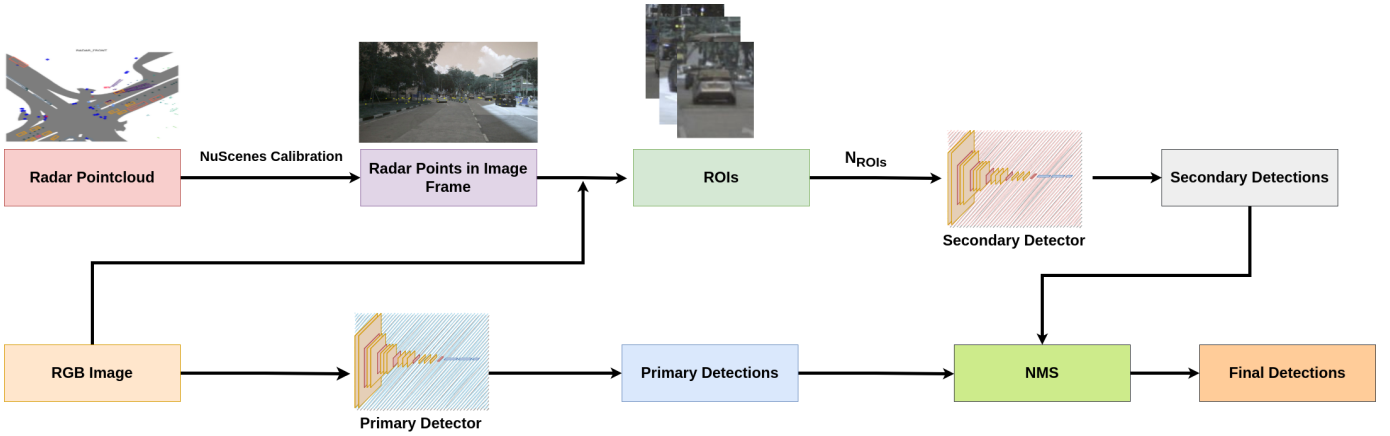


Fig. 2: Algorithmic pipeline of Proposed Fusion System



Fig. 3: a.) Yellow points in the image show radar points mapped to the camera image, b.) Radar based proposals generated for secondary detector



(a) 2D annotations in nuScenes (b) 2D annotations labelled by us

Fig. 4: Comparison of Nuscenes 2D annotations and our labelled annotations for images from front camera

to the secondary detector to generate secondary detections. The secondary detections are then merged with the primary detections to generate final detections. The use of radar data ensures that we do not create redundant proposals for detection with no objects. Unlike tiling methods, this method generates proposals in a dynamic fashion. The overall computational cost of the system will depend on the choice of lightweight detectors and the number of radar points. For automotive radars like Aptiv ESR 2.5 [27] that detect less than 64 objects at any timestamp, the maximum computational overload will be 64 times the GFLOPs of the lightweight detector. For a suitable choice of lightweight detector, this could be very well managed by a resource efficient system.

1) *Radar Object Proposals*: Detected objects by automotive radars are reported as 3D points in bird's eye view. In addition to position and depth, radars also report the radial velocity of the moving objects. For our method, we parameterize the radar detection as $D = (x, y, z)$ and treat every detection as stand-alone detection. As a pre-processing step, we perform spatial alignment of radar data into the camera's coordinate system. The nuScenes dataset provides us with the necessary calibration tools for mapping radar points to the egocentric and camera frame. When mapped onto the camera frame, radar detections point to the detected objects in the frame. Even though not all the objects are detected by radar,

detections include most of the objects in long range detected with high confidence. Each radar point in camera frame is parametrized as $P = (cx, cy)$. We treat this as the approximate location of an object and draw a 2D anchor of predefined size for every point with P as the center. Figure 3a shows radar points in yellow mapped to the camera frame while ROIs generated using radar points are shown in red boxes in figure 3b.

2) *Object Detection*: The secondary detector is responsible for detecting the objects in the ROIs generated by radar object proposal network. For each radar point, the region bounded by the anchor box is cropped from the image and sent to a lightweight detector. For each image, we generate n ROIs for secondary detection, where n is the total number of radar points in the given frame. All the detections for n ROIs are aggregated with detections by the primary detector generated by passing the full image. Finally, we perform Non-maximum Suppression(NMS) on the aggregated detections to filter out any double detections.

TABLE II: FLOPs of Object Detectors

Detector	Image size	GFLOPs
yolov3-spp	416	66.4
	640	157
	1080	447
	1900	1384.6
tiny-yolov3	200	1.3
	300	2.9
	400	5.2
	600	14.1
SSDlite	200	0.20
	300	0.43
	400	0.74

III. EXPERIMENTAL RESULTS

A. Dataset

We test our proposed fusion method on the validation set of the nuScenes [20] dataset that has synchronized data collected from an autonomous vehicle sensor suite of 6 cameras, 5 radars, and 1 lidar, all with a full 360-degree field of view. Since nuScenes has 3D annotations, we first convert these 3D annotations to 2D annotations and merge all relevant classes into 6 classes: car, truck, bus, pedestrian, bicycle, and motorcycle. For our evaluation purposes, we discard highly occluded objects from ground truths annotated in 3D. As shown in figure 4, we observe that many of the far-away objects in the scenes did not have any annotations. This is due to the fact that objects that are not covered with at least one lidar or radar point are discarded by nuScenes even though they were captured by RGB cameras. To overcome this, we annotate a small sample of images manually from the *mini-val* split of nuScenes. Our dataset contains 396 images and 3777 annotations with annotated classes of: 'cars,' 'pedestrian', 'truck', 'trailer', 'bus', 'cycle', and 'motorcycle'. The predicted detections are compared against our manually annotated dataset since it has more labels as compared to nuScenes 2D annotations.

B. Object Detection network

We use yolov3-spp, tiny-yolov3 and SSDlite as our primary and secondary object detector for our experiments. It is important to note here that, this approach is applicable to any combination of primary and lightweight secondary detectors to obtain significant detection improvement at low computational power. All the object detectors were trained on the COCO dataset [28] and detection with classes belonging to 'Car', 'Person', 'Bicycle', 'Motorcycle', 'Bus' and 'Truck' considered for evaluation. We compare our fusion system with the detections from the primary detectors. We used PyTorch to implement our system and all the experiments were conducted on a setup with two Nvidia 1080Ti GPUs.

C. Metrics For Evaluation

To compare the detection ability of different object detection systems, we use Recall and the number of False Negatives as our metric. Recall measures the number of correctly detected

TABLE III: Value Table.

Name	Value
α^*	20mJ/frame
β^1	0.92J/frame
γ^*	3.9mJ/Mb
f_s	34.5Mb
f_{ps}	20
EE_{hw}	3.08 TOPS/W

* Values adapted from [29]

¹ Values calculated from Delphi ESR-2.5 datasheet [27] with max frame-rate=13fps,

objects over the number of objects in the ground truth. Following is the equation for Recall:

$$Recall = \frac{TruePositives}{TruePositives + FalseNegatives} \quad (1)$$

For comparison between different detectors based on the computation overhead, we compute the number of floating operations executed per second. Table II shows the comparison of computational overhead in GFLOPs for yolov3-spp, tiny-yolo and SSDlite. We also compute the total energy consumed per frame for different object detectors. This includes energy consumption for sensor activations, data transfer of captured frames and computational expenses due to object detectors. Based on [30], equations for resource consumption are described below:

$$Energy = \alpha + \beta + \gamma * f_s + \frac{(CL_{pd} + CL_{sd} * N^{ROIs}) * f_{ps}}{EE_{hw}} \quad (2)$$

Here, α , β are the per frame sensor's data capture energy for RGB cameras and radar respectively while γ is the energy spent on transferring captured frames to the perception engine of the system. CL_{pd} and CL_{sd} are the computational overhead of the primary and secondary object detector respectively. N^{ROIs} represent the number of ROIs created by the radar proposal network per frame that are processed by the secondary detector. f_s is the combined frame size memory for the radar pointcloud and camera image. We fix the nuScenes frame rate(f_{ps}) to 20 for our experiments. UNPU [31] is used as the DNN accelerator to estimate the computational energy required to run the object detector and EE_{hw} denotes the energy efficiency of our DNN accelerator. For our calculations, we assume that our system has an automotive radar of 77GHz frequency and an RGB monocular camera that are always turned on. Table III shows the values of the variables in equation 2 used for our evaluation.

D. Hyperparameter Study

Our proposed algorithm's performance depends on the choice of ROI size of the proposal and input image size for the lightweight detector since these determine the effective receptive field of the objects in ROIs. A large ROI proposal will decrease the effective stimuli of the object thereby leading to a missed detection while a small ROI may crop some pixels of the object necessary for the detection. The receptive field

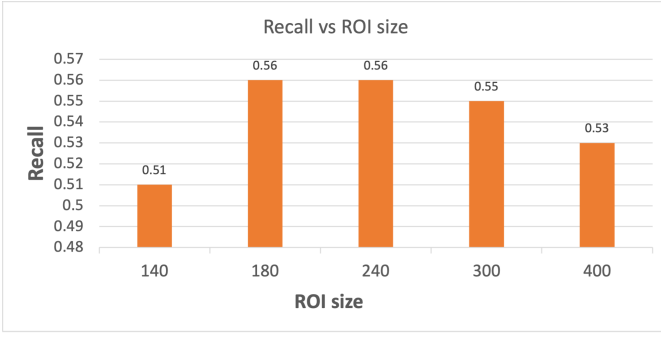


Fig. 5: ROIs size vs Recall comparison with yolov3-spp as primary detector and tiny-yolov3 as secondary detector



Fig. 6: Multiple detection for small ROI sizes not removed after NMS

of the object increases as the input size of the detector is increased, however it leads to an increase in the computational overhead of the network. Hence, it is important to find appropriate ROI and input image size for the secondary detector to balance the performance and memory footprint of the network.

1) *Effect of ROI size on recall*: We compared the performance of our fusion method for different input image sizes of the secondary detector and ROI size for secondary detections. Figure 5 shows the recall for different ROIs sizes. We performed the experiments with yolov3-spp as the primary detector and tiny-yolov3 as the secondary detector with input sizes of 416 and 300 respectively and a low IoU of 0.1 to recover as many false negatives as possible. It is to be noted that changing the ROI size has no effect on overall energy consumption as the energy consumption only depends on the input image sizes of the detectors. We find the highest recall for ROI sizes of 180 and 240 and the performance degrades if the ROI size is further increased. For small ROI sizes, we observe an increase in false positives due to multiple detections of nearby objects as shown in figure 6.

2) *Effect of secondary detector's input size on recall and computational overhead*: Table IV shows the performance and average GFLOPs per frame for different input sizes of the secondary detector tiny-yolov3 while the input size of the primary detector was fixed to 416. Based on our previous study, we fix the ROI size to 240 for this experiment. The recall is highest for the image size of 300 and we observe a

TABLE IV: Resource and recall comparison for different input sizes of the secondary detector

Image size	Recall	GFLOPs
200	0.53	131.4
256	0.53	171.4
300	0.56	211.4
350	0.51	266.4
416	0.52	346.4

TABLE V: Performance and computational overhead for different fusion systems

Mode	P det	Sec det.	Rcll \uparrow	Prcn \uparrow	FN \downarrow	TE \downarrow	GF \downarrow
Fusion	yolov3-spp	tiny-yolov3	0.51	0.68	1835	1.78	211.4
Fusion	yolov3-spp	yolov3-spp	0.63	0.75	1398	12.03	1791.4
Fusion	tiny-yolov3	tiny-yolov3	0.55	0.81	1833	1.50	150.6
Fusion	yolov3-spp	SSDlite	0.51	0.67	1851	1.32	87.9
Fusion	SSDlite	SSDlite	0.48	0.69	1978	1.10	22.3

Pdet=Primary detector, *Secdet*=Secondary detector, *Rcll*=Recall, *Prcn*=Precision, *FN*=False Negatives, *TE*=Avg. Energy(J) per frame, *GF*= avg GFLOPs/frame

decrease in the recall if we increase the image size beyond 300. Increasing the input size for the secondary detector with small input ROIs will increase the upscaling of the ROI before it is processed by the object detector and lead to an increase in noisy detections. The memory footprint of the network increases as the input size is increased. Based on the recall numbers and GFLOPs for the network, we choose an image size of 300 for the secondary detector. For all our further experiments, we fix the input image size of the secondary detector to 300 and the ROI size to 240.

E. Evaluation

1) *Experiments with different detectors*: Table V shows the performance of the fusion algorithm using different primary and secondary object detectors. The table shows the Average Recall (AR), Average Precision (AP), False Negatives, Total Energy consumption per frame and average GFLOPs per frame for the object detection task with an IoU of 0.4. The image sizes for the primary detector and the secondary detector are kept to 416 and 300 respectively with an ROI size of 240. According to Table V, we get the highest recall for the system with yolov3-spp as both primary and secondary detector, however, it requires memory of 1791.4 GFLOPs per frame which is very high for a system with limited

TABLE VI: Comparison of our fusion system with baselines

Mode	P det.(im sz)	Sec det.	Rcll \uparrow	Prcn \uparrow	FN \downarrow	TE \downarrow	GF \downarrow
Fusion	yolov3-spp(416)	SSDlite	0.51	0.67	1851	1.32	87.9
Fusion	SSDlite (416)	SSDlite	0.48	0.69	1978	1.10	22.3
Base Network							
Base	yolov3-spp (416)		0.42	0.92	2205	1.24	66.4
Base	yolov3-spp (1080)		0.53	0.93	1769	2.48	447.4
Prior Work							
Fusion	BIRANet-FFPN		0.53	0.73	1762	1.71	207

Pdet=Primary detector, *Secdet*=Secondary detector, *imsz*=Input image size for detector, *Rcll*=Recall, *Prcn*=Precision, *FN*=False Negatives, *TE*=Avg. Energy(J) per frame, *GF*= avg GFLOPs/frame

computational resources. Fusion networks with tiny-yolov3 and SSDlite have similar performance in terms of average recall, however there is a big difference between their memory requirements. Network with yolov3 as primary and tiny-yolov3 as secondary detector requires more than twice the memory that the fusion system of yolov3 and SSDlite as primary and secondary detector respectively. Hence, we choose SSDlite as our secondary detector due to its low complexity and memory footprint. For SSDlite systems, yolov3 as the primary detector has the best recall however it requires nearly four times more computational power than the framework with SSDlite as the primary detector. In a system with very low computational power, a framework with SSDlite as both primary and secondary detector could be chosen over the yolov3-SSDlite framework with a slight decrease in detection accuracy. The framework with SSDlite as the primary detector will be referred to as 'SSDlite-SSDlite' while the framework with yolov3 as the primary detector will be 'yolov3-SSDlite.'

2) *Comparison with baselines:* In Table VI, we compare the performance of our SSDlite fusion systems with two single yolov3-spp networks operating at input image sizes of 416 and 1080. The yolov3 network with an input size of 1080 has a bigger receptive field for small objects and hence scores better recall than its counterpart with an input size of 416. Our both fusion systems (yolov3-SSDlite and SSDlite-SSDlite) outperform the baseline yolov3 with an input size of 416 with an improvement of 21% and 14% in the recall respectively. The single yolov3 detector with an input size of 1080 performs slightly better than our fusion systems however requires nearly 5 and 20 times more resources than our yolov3-SSDlite and SSDlite-SSDlite fusion systems respectively. This demonstrates the high performance of our fusion systems while having very low memory requirements.

We also evaluated BIRANet [19] on our dataset and observed only 4% and 10% increase in recall compared to our SSDlite-SSDlite and Yolov3-SSDlite fusion systems respectively even though it uses high performing Faster R-CNN with a feature pyramid network for detection. The memory requirements for BIRANet are also very high compared to our fusion systems, requiring almost 9 times computational memory compared to our SSDlite-SSDlite fusion system. We also plot per frame recall for BIRANet, baseline yolov3 with 1080 input size and yolov3-SSDlite fusion system in figure 7. We observe that our fusion system has very a similar recall as compared to other analyzed networks over the sequence. Thus our system is most suitable for deployment in real world resource efficient systems with the promise of better performance at low memory consumption.

Figure 8 shows the variation of memory requirements with the RGB frames for our fusion system with yolov3 and SSDlite. Unlike the tiling methods where a fixed number of proposals are created, our fusion system's number of proposals depend on detection made by radars. Hence the computational requirements change dynamically depending on the radar detections. This behavior is captured in figure 8. This ensures that the energy consumption is kept low for the dynamic scenes

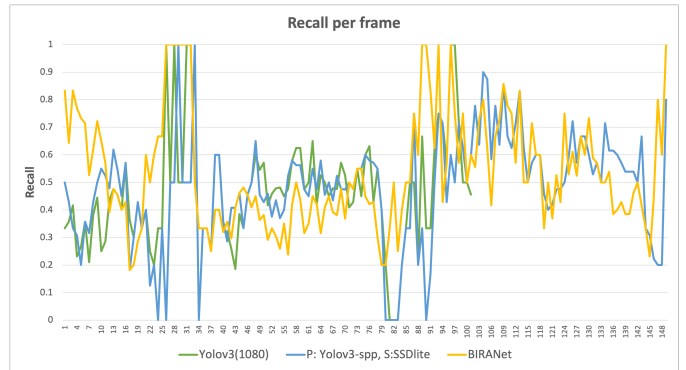


Fig. 7: Recall per frame for different detectors

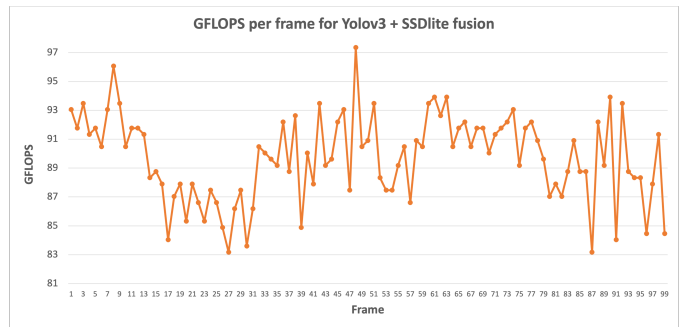


Fig. 8: GFLOPs per frame for fusion system with yolov3 and SSDlite as primary and secondary detector respectively

with very few objects in the frame.

The effect of object size on the detection performance of our system is analysed in figure 9. The y-axis in the figure represents the number of true positives and the x-axis represents the area of the detected true positive objects. We use SSDlite as the secondary detector and yolov3-spp as the primary detector with other parameters as mentioned above. In general, the performance of the fusion system and baseline are comparable for large objects. However, we see a significant increase in true positives with an area less than 1000 $pixel \times pixel$ for our fusion system as compared to the baseline primary detector.

Figure 10 shows the qualitative results of our fusion system with yolov3 as the primary detector and SSDlite as the secondary detector. The results support that our method performs very good in detecting small objects as well as the objects in low lightening or contrast regions. The image in the fourth row belongs to a dark sequence in nuScenes and our detectors have never seen night time sequences during training making object detection harder.

IV. CONCLUSION

Deep convolutional network based object detectors often fail in detecting small objects when operating at a fixed size input. The lack of distinctive semantic features for the object and the mixing of background features when passed through the convolution network makes the small object detection problem

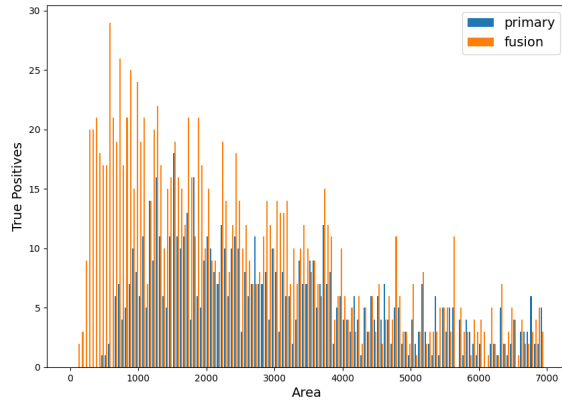


Fig. 9: Detection performance with respect to object area

very challenging. In this work, we have shown how radar could be used to create object proposals which when passed through a lightweight detector could help in the detection of small objects missed by the RGB detector. The proposed architecture uses a primary and a lightweight detector with low computational overhead to detect objects. The radar pointcloud is used to generate object proposal regions and these proposals are fed into the secondary detector to generate secondary detections. Detections generated with the primary detector with the full image as input are fused with the secondary detections via NMS. Our proposed fusion algorithm has the merits of high performance at longer distances, low computational requirements, high reliability and robustness. Experiments on our annotated dataset show that our proposed SSDlite-SSDlite fusion method outperforms baseline primary yolov3 detector with a 14% increase in recall while having a very small computational overhead of 22.3 GFLOPs as opposed to the baseline's 66.4 GFLOPs.

REFERENCES

- [1] Ross B. Girshick, Jeff Donahue, Trevor Darrell, and Jitendra Malik. Rich feature hierarchies for accurate object detection and semantic segmentation. *CoRR*, abs/1311.2524, 2013.
- [2] Ross B. Girshick. Fast R-CNN. *CoRR*, abs/1504.08083, 2015.
- [3] Shaoqing Ren, Kaiming He, Ross B. Girshick, and Jian Sun. Faster R-CNN: towards real-time object detection with region proposal networks. *CoRR*, abs/1506.01497, 2015.
- [4] Zhiqiang Shen, Zhuang Liu, Jianguo Li, Yu-Gang Jiang, Yurong Chen, and Xiangyang Xue. DSOD: learning deeply supervised object detectors from scratch. *CoRR*, abs/1708.01241, 2017.
- [5] Wei Liu, Dragomir Anguelov, Dumitru Erhan, Christian Szegedy, Scott E. Reed, Cheng-Yang Fu, and Alexander C. Berg. SSD: single shot multibox detector. *CoRR*, abs/1512.02325, 2015.
- [6] Joseph Redmon and Ali Farhadi. Yolov3: An incremental improvement. *CoRR*, abs/1804.02767, 2018.
- [7] fahriye Unel, Burak Ozkalayci, and Cevahir Cigla. The power of tiling for small object detection. 06 2019.
- [8] Kshitiz Garg and Shree K. Nayar. When does a camera see rain. In *in Proc. ICCV 2005*, pages 1067–1074, 2005.
- [9] Rita Spinneker, Carsten Koch, Su-Birm Park, and Jason Yoon. Fast fog detection for camera based advanced driver assistance systems. pages 1369–1374, 10 2014.
- [10] Pei Sun, Henrik Kretschmar, Xerxes Dotiwalla, Aurelien Chouard, Vijaysai Patnaik, Paul Tsui, James Guo, Yin Zhou, Yuning Chai, Benjamin Caine, Vijay Vasudevan, Wei Han, Jiquan Ngiam, Hang Zhao, Aleksei Timofeev, Scott Ettinger, Maxim Krivokon, Amy Gao, Aditya Joshi, Yu Zhang, Jonathon Shlens, Zhifeng Chen, and Dragomir Anguelov. Scalability in perception for autonomous driving: Waymo open dataset. *CoRR*, abs/1912.04838, 2019.
- [11] Andreas Geiger, Philip Lenz, Christoph Stiller, and Raquel Urtasun. Vision meets robotics: The kitti dataset. *International Journal of Robotics Research (IJRR)*, 2013.
- [12] Adam Ziebinski, Rafal Cupek, Damian Grzechca, and Lukas Chrusczyk. Review of advanced driver assistance systems (adas). In *AIP Conference Proceedings*, volume 1906, page 120002. AIP Publishing LLC, 2017.
- [13] Ricardo Chavez-Garcia, Julien Buret, Trung-Dung Vu, and Olivier Aycard. Frontal object perception using radar and mono-vision. 06 2012.
- [14] Jianmin Duan, Lu Ren, Longjie Li, and Dan Liu. Moving objects detection in evidential occupancy grids using laser radar. In *2016 8th International Conference on Intelligent Human-Machine Systems and Cybernetics (IHMSC)*, volume 02, pages 73–76, 2016.
- [15] Takeo Kato, Yoshiki Ninomiya, and Ichiro Masaki. An obstacle detection method by fusion of radar and motion stereo. *SICE 2003 Annual Conference (IEEE Cat. No.03TH8734)*, 1:689–694, 2003.
- [16] Charles R. Qi, Hao Su, Kaichun Mo, and Leonidas J. Guibas. Pointnet: Deep learning on point sets for 3d classification and segmentation, 2017.
- [17] Wei-Yu Lee WeiYuLee, UGentbe Ljubomir Jovanov LjubomirJovanov, and UGentbe Wilfried Philips WilfriedPhilips. Semantic-Guided Radar-Vision Fusion for Depth Estimation and Object Detection. 2021.
- [18] Vijay John and Seiichi Mita. Rvnet: Deep sensor fusion of monocular camera and radar for image-based obstacle detection in challenging environments. In *PSIVT*, 2019.
- [19] Ritu Yadav, Axel Vierling, and Karsten Berns. Radar+rgb attentive fusion for robust object detection in autonomous vehicles. *CoRR*, abs/2008.13642, 2020.
- [20] Holger Caesar, Varun Bankiti, Alex H. Lang, Sourabh Vora, Venice Erin Liong, Qiang Xu, Anush Krishnan, Yu Pan, Giancarlo Baldan, and Oscar Beijbom. nuscenes: A multimodal dataset for autonomous driving, 2020.
- [21] Andrew Howard, Mark Sandler, Grace Chu, Liang-Chieh Chen, Bo Chen, Mingxing Tan, Weijun Wang, Yukun Zhu, Ruoming Pang, Vijay Vasudevan, Quoc V. Le, and Hartwig Adam. Searching for mobilenetv3. *CoRR*, abs/1905.02244, 2019.
- [22] Songtao Liu, Di Huang, and Yunhong Wang. Receptive field block net for accurate and fast object detection. *CoRR*, abs/1711.07767, 2017.
- [23] Andrew G. Howard, Menglong Zhu, Bo Chen, Dmitry Kalenichenko, Weijun Wang, Tobias Weyand, Marco Andreetto, and Hartwig Adam. Mobilenets: Efficient convolutional neural networks for mobile vision applications. *CoRR*, abs/1704.04861, 2017.
- [24] Xizhou Zhu, Han Hu, Stephen Lin, and Jifeng Dai. Deformable convnets v2: More deformable, better results. *CoRR*, abs/1811.11168, 2018.
- [25] Simon Chadwick, Will Maddern, and Paul Newman. Distant vehicle detection using radar and vision. *CoRR*, abs/1901.10951, 2019.
- [26] Bin Yang, Runsheng Guo, Ming Liang, Sergio Casas, and Raquel Urtasun. Radarnet: Exploiting radar for robust perception of dynamic objects. *CoRR*, abs/2007.14366, 2020.
- [27] Radar comparison chart, <https://autonomoustuff.com/radar-chart>.
- [28] Tsung-Yi Lin, Michael Maire, Serge Belongie, Lubomir Bourdev, Ross Girshick, James Hays, Pietro Perona, Deva Ramanan, C. Lawrence Zitnick, and Piotr Dollár. Microsoft coco: Common objects in context, 2015.
- [29] Kruttidipta Samal, Hemant Kumawat, Priyabrata Saha, Marilyn Wolf, and Saibal Mukhopadhyay. Task-driven rgb-lidar fusion for object tracking in resource-efficient autonomous system. *IEEE Transactions on Intelligent Vehicles*, pages 1–1, 2021.
- [30] Kruttidipta Samal, Marilyn Wolf, and Saibal Mukhopadhyay. Introspective closed-loop perception for energy-efficient sensors. In *2021 17th IEEE International Conference on Advanced Video and Signal Based Surveillance (AVSS)*, pages 1–8, 2021.
- [31] Jinmook Lee, Changhyeon Kim, Sanghoon Kang, Dongjoo Shin, Sangyeob Kim, and Hoi-Jun Yoo. Unpu: A 50.6tops/w unified deep neural network accelerator with 1b-to-16b fully-variable weight bit-precision. In *2018 IEEE International Solid - State Circuits Conference - (ISSCC)*, pages 218–220, 2018.



(a) Detections by Fusion method

(b) Detections by Primary Detector

Fig. 10: Qualitative results of our fusion algorithm